Surface modification of an amorphous Si thin film crystallized by a linearly polarized Nd:YAG pulse laser beam

Susumu Horita,[a] Hirokazu Kaki, and Kensuke Nishioka
Japan Advanced Institute of Science and Technology, 1-1 Asahidai, Nomi, Ishikawa 923-1292, Japan

(Received 5 November 2006; accepted 16 May 2007; published online 2 July 2007)

Amorphous Si films of 60 and 10 nm thick on glass substrates were irradiated by a linearly polarized Nd:YAG pulse laser with the wavelength $\lambda=532$ nm at the incident angle $\theta_i=0$. The surface of the irradiated 60-nm-thick film had both periodic ridges perpendicular to the electric field vector $\boldsymbol{E}$ and aperiodic ridges roughly parallel to $\boldsymbol{E}$, where the spatial period of the periodic ridges was almost λ. From the continuous 10-nm-thick film, the separate rectangular Si islands were formed with a periodic distance of λ, with the edges parallel or perpendicular to $\boldsymbol{E}$. When θ_i was increased from normal incidence of the *s*-polarized beam for a 60-nm-thick film, the aperiodic ridges were reduced while the periodic ridges were still formed. For a 10-nm-thick film, the Si stripes were formed perpendicular to $\boldsymbol{E}$, using the *s*-polarized beam at $\theta_i=12°$. In order to investigate the mechanisms of the surface modifications of, in particular, aperiodic ridges, islands, and stripes, we improved the previous theoretical model of the periodic distribution of the beam energy density (periodic E-D) generated by irradiation of the linearly polarized laser beam, taking account of the multireflection effect in the Si film which is semitransparent for λ. Further, the calculated E-D was corrected with respect to the thermal diffusion in the irradiated Si film. The calculation results show that the two-dimensional E-D consists of a constant or a dc term and a sinusoidal or an ac term which contains various spatial periods. The multireflection effect strongly influences the amplitude and phase of every ac term, which means that the amplitude and phase depend on the film thickness. The thermal diffusion during the heating of the irradiated film greatly reduces the amplitudes of the ac terms with periods below the thermal diffusion length. The theoretical calculation showed that, by increasing θ_i, the temperature distribution in the irradiated Si film was changed from two-dimensional toward one-dimensional, which can explain the above experimental results reasonably. © *2007 American Institute of Physics*. [DOI: 10.1063/1.2751085]

I. INTRODUCTION

Low-temperature polycrystalline silicon (LT poly-Si) thin film transistors (TFTs) are widely used for various applications. Among many fabrication methods of the LT poly-Si film, the pulse laser annealing (PLA) method, in which a Si film deposited on an inexpensive glass substrate is melted by pulse laser irradiation for quick crystallization, is more effective in producing crystallized Si films with larger grain for high carrier mobility.[1,2] However, ideal TFTs require active regions entirely free of grain boundaries which reduce carrier mobility, cause the threshold voltage to fluctuate, and increase the off current of the transistor. In order to suppress the generation of grain boundaries, it is necessary to control the temperature distribution in the irradiated Si film so as to reduce random nucleation and unify the solidification direction of the molten Si. For this requirement, some researchers have proposed modulated PLA methods using an absorption layer,[3,4] a prepatterned Si layer,[5] and so on[6–9]. The interference PLA methods using a beam splitter[10] or a phase-shift mask[11,12] have also been developed. However, the former require other fabrication processes in addition to crystallization, and the latter need additional optical components and optical alignment before crystallization.

We have reported that, using a spatially periodic distribution of the beam energy density (periodic E-D) induced spontaneously by irradiation of a linearly polarized laser beam, we can control the location of grain boundaries in a Si film crystallized on a Pyrex glass substrate.[13,14] We used a Nd:YAG (yttrium aluminum garnet) pulse laser with the wavelength λ of 532 nm. The first advantage of this method over the above conventional ones is that there is no requirement for additional fabrication processes or optical components. Therefore, the process cost and time of our method are much lower than those of the other methods.

For more than 25 years, it has been well known that irradiation of the linearly polarized laser beam on the surface of a material generates a periodic E-D which, as a result, produces the distinctly periodic surface structures of bulk materials such as metal,[15,16] semiconductor,[16–25] and polymer films.[26,27] The initial surface of a material before irradiation has no periodic roughness but a smooth surface. However, microscopically, the actual initial surface has a random roughness composed of low surface gratings spaced at varying intervals. Therefore, the roughness may have a special periodic component to produce and modify a diffracted beam traveling on the surface. This modification results from the interaction of waves between the primary incident beam and the diffracted beams, so that a periodic E-D is produced. If the surface roughness of the special component is increased

[a]Electronic mail: horita@jaist.ac.jp; FAX: +81-761-51-1149.

only slightly at the first pulse irradiation due to a faint amplitude of the periodic E-D, the increased surface roughness leads to an increase in the diffracted beam intensity at the following irradiation, which leads to an increase of the modulation in the E-D of the primary incident beam. Thus, the modification of the surface roughness and that of the E-D enhance each other in a positive feedback loop.[28] The details are mentioned later in Sec. II.

In our case, the generated periodic E-D has a one-dimensional function such as $\cos(x)$ on the irradiated surface of the Si film (x-y plane). The maximum or minimum energy density lines are parallel to one another along the y direction, and are separated by a regular periodic distance of near λ (normal incident case). Also, they are perpendicular to the electric field vector $\boldsymbol{E}$ of the incident beam. The periodic E-D produces the spatially periodic distribution of temperature (periodic T-D) on the irradiated Si film, and this periodic T-D is similar to the periodic E-D. At each line region of the minimum temperature in the periodic T-D, nucleation of Si occurs and the solidification extends to both of the nearest neighboring high-temperature regions. Then, the two adjoining solidification fronts which proceed toward opposite directions collide each other at the periodic line region of the maximum temperature. So, grain boundaries are generated along the periodic collision lines perpendicular to $\boldsymbol{E}$ or along the y direction. As a result, over the whole crystallized Si film, the location of the grain boundary generation is controlled to be periodically perpendicular to $\boldsymbol{E}$ with the spatial period $\Lambda \approx \lambda$ (normal incident case). Here, we should note that the actual E-D and T-D are not one-dimensional but two-dimensional, which is mentioned in more detail in Sec. V later. Also, being accompanied with the alignment of a grain boundary due to the periodic E-D, a periodic surface structure is formed on the crystallized film. The periodic ridges have already been reported on a Si film crystallized on a glass substrate.[13,14,29–33] The ridges are inevitably formed along the lines of the periodic grain boundaries caused by the collision of the solidification fronts. Fork *et al.* have proposed a quantitative model of formation of the ridge or hill, in which a substantial mass transport of liquid Si is caused by the laterally advancing grains through the denser liquid.[30] Since the vertices of the periodic ridges are located around the grain boundaries, the grating vector $\boldsymbol{k}_g$ of the periodic structure is parallel to the surface component of $\boldsymbol{E}$, as shown schematically in Fig. 1(a). In addition to the periodic ridges, we observed aperiodic ridges which are slightly curved, roughly perpendicular to the periodic ridges, and separated by irregular distances of a few to several micrometers. They were also observed even on the surfaces of bulk materials in the photographs included in some previous research papers, but they were not mentioned in the texts of those papers.[16,34] The aperiodic ridges are unfavorable for TFT devices since they hinder uniform performance. In order to suppress the formation of the aperiodic ridge for a 60-nm-thick amorphous Si (a-Si) film, we increased the incident angle θ_i from normal to 20° with an s-polarized beam, and performed crystallization. As a result, the generation of the aperiodic ridges was suppressed effectively, and the periodic ridges perpendicular to $\boldsymbol{E}$ with $\Lambda \approx \lambda$ were still formed in the same way as in the normal incident case,[35] as shown in Fig. 1(b).

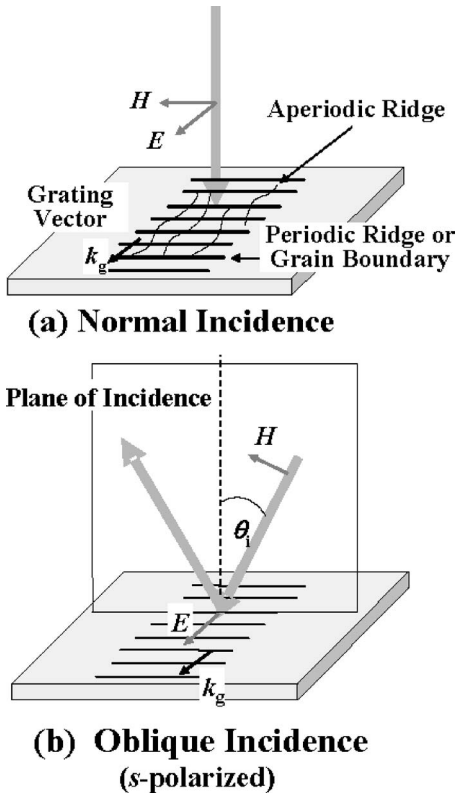

FIG. 1. Schematic drawings of the surface of the sample irradiated by a linearly polarized laser beam at (a) normal incidence and at (b) oblique incidence with s polarization. The fine periodic ridges are formed perpendicular to the electric field vector $\boldsymbol{E}$, and the aperiodic ridges are formed roughly parallel to $\boldsymbol{E}$. $\boldsymbol{k}_g$ is the grating vector of the fine periodic ridge, and $\boldsymbol{H}$ is the magnetic field vector. The height of the aperiodic ridges is reduced by increasing the incident angle θ_i.

The surface ridges are shaped during the molten Si solidification process, which depends mostly on the molten Si T-D induced by the periodic E-D. Some researchers have analyzed the periodic E-D theoretically, and explained the formation mechanism of the periodic ridges or periodic structure successfully using their analysis results.[22–25,36,37] Although the E-D was calculated under the condition of a constant temperature, e.g., room temperature or melting temperature, and the melting and solidification processes were not taken into account, it contained enough useful information for qualitative explanation. However, the calculated periodic E-D has not been able to explain the formation and suppression of the aperiodic ridge.

So, in this paper, in order to find clues about the mechanisms of surface modification, i.e., the formation and suppression of the aperiodic ridges, we present a theoretical analysis of the periodic E-D on the irradiated surface of the Si film on the glass substrate. Although this analysis is based on the of Guosheng *et al.* theoretical model,[37] we take the multirefection effect in a semitransparent Si film into account. This is because the previous analyses are only for bulk or opaque material, but not for semitransparent materials such as Si thin film. Then, we improve the previous model for its application to a Si thin film thinner than the absorption

length of the laser beam at 532 nm. Furthermore, we correct the calculated values of the theoretical E-D by considering thermal diffusion during irradiation. Some papers mention that, in the case of pulsed-laser-induced periodic structures, the heat flow is negligible and the structure formation is determined solely by the periodic E-D.[25,36] However, the periodic T-D which determines predominantly the periodic structure on the Si film is strongly dependent on not only periodic E-D but also on the thermal property of the irradiated material because the thermal diffusion length of Si, e.g., ~100 nm for 1 ns, is longer than a film thickness of ~50 nm. Next, we show the experimental results of the oblique incident case with an *s*-polarized beam for 60-nm-thick *a*-Si films, compared with the normal incident case. Also, we show the results for 10-nm-thick *a*-Si films crystallized by *s*-polarized pulse beams with oblique and normal incident angles. For thinner films, the modification of the surface morphology after melting is more influenced by E-D. In fact, we show here that the morphology of the crystallized 10-nm-thick Si film is completely different from the case of the 60-nm-thick film, and depends strongly on the incident angle. Regarding the 10-nm-thick film, irradiations at normal incidence and oblique incidence produced many separated Si islands and Si stripes, respectively. Finally, we discuss the surface modification mechanisms of the formation and suppression of aperiodic ridges on the 60-nm thick film, based on the theoretical calculation results of the E-D, which are taken account of both the effects of multireflection and thermal diffusion, as well as discuss the mechanisms of Si island and stripe formation from the 10-nm-thick film.

II. THEORETICAL MODEL

A. Basic bulk case

The first-order theoretical (and experimental) synchronism condition for the periodic surface structure formation is

$$\boldsymbol{k}_0 \sin\theta_i \pm \boldsymbol{k}_\mathbf{g} = \boldsymbol{k}_\mathrm{s} \tag{1}$$

in the irradiated surface plane, where $\boldsymbol{k}_0$ is the incident beam wave vector, $\boldsymbol{k}_0 \sin\theta_i$ is the beam wave vector component of the incident beam on the surface, and $\boldsymbol{k}_s$ is the wave vector of the first-order surface scattering beam.[28] It has been reported that most $\boldsymbol{k}_\mathbf{g}$ of semiconductors and metals run parallel to the surface component of the $\boldsymbol{E}$ of the primary incident beam,[16,20,21] which means that the diffraction efficiency parallel to $\boldsymbol{E}$ is much greater than that parallel to the magnetic field vector $\boldsymbol{H}$. Due to the property of diffraction efficiency and Eq. (1), at some incident angle θ_i for *p*-polarized beam, the $\boldsymbol{k}_\mathbf{g}$ is parallel to both the plane of incidence and the surface component of $\boldsymbol{E}$, and the ridge of the periodic surface structure has the spatial period of $\Lambda \approx \lambda/[n_0(1 \pm \sin\theta_i)]$, where n_0 is the refractive index in the incident atmosphere. For the *s*-polarized beam with θ_i, the $\boldsymbol{k}_\mathbf{g}$ is parallel to $\boldsymbol{E}$ but perpendicular to the plane of incidence, and the period is $\Lambda \approx \lambda/(n_0 \cos\theta_i)$.

The E-D on the bulk material and opaque thin film for the laser beam can be calculated, based on the theoretical report of Guosheng *et al.* on the laser beam E-D generated on the periodically corrugated surface of the sample.[37] The corrugated vacuum-solid interface is described by $z(x) = -h\cos(2\pi x/\Lambda)$, where h is the amplitude of the corrugation, the z axis is outward perpendicular to the macroscopic surface, and the x axis is perpendicular to the corrugation.

The Poynting vector modulated by the diffraction can be calculated from the standard diffraction theory and Maxwell's equations, and the normal component of the time-average Poynting vector P_n just inside the medium can be expressed approximately as

$$P_n \cong P_0\left[1 + A\cos\left(\frac{2\pi}{\Lambda}x - \phi_p\right)\right], \tag{2}$$

where $P_0 > 0$ is the dc or average component, $A > 0$ is the ac amplitude ratio, and ϕ_p is the phase difference between the sinusoidal surface corrugation and P_n. The ac term comes from the interaction between waves of zeroth order and first order, and is proportional to h. The details are mentioned in Ref. 37. In this equation, the physical meaning of $\phi_p = \pm 180°$ corresponds to the beam energy being absorbed more in the "hills" than in the "valleys" of the corrugation, while $\phi_p = 0$ corresponds to the opposite situation. At $\phi_p = \pm 180°$, since the hills or ridge regions are heated more than the valley regions, and the higher temperature molten regions solidify later,[30] the height of the ridges is increased after solidification. Thus, due to this increased height of h, the ac component amplitude of P_n at next irradiation is enhanced, so that more distinctly periodic E-D can be generated. This means that the condition $\phi_p = \pm 180°$ causes a positive feedback loop for periodic ridge formation, and is favorable for controlling the grain boundary location in the crystallization method. On the contrary, $\phi_p = 0$ is unfavorable for forming the periodic ridge and controlling the grain boundary location because the valley regions are more heated. Therefore, the irradiated Si film surface becomes flattened and the ac component amplitude of P_n is reduced, which results in the disappearance of periodic E-D.

B. Semitransparent thin film case

Because the absorption length of 532 nm of Si at room temperature is about 1100 nm[38] which is much greater than the typical thickness of Si film in TFT, <100 nm, we must take account of the multireflection in the Si film between the interfaces of the incident atmosphere/Si and Si/substrate. In the case of excimer laser annealing, no multireflection is considered because of a much shorter absorption length, e.g., 6.76 nm at 308 nm.[38] It should be noted that the analysis of Guosheng *et al.* is performed just on the surface of the bulk medium, and that the amplitude ratio A and phase ϕ_p in Eq. (2) are dependent on the refractive indices of the incident atmosphere and irradiated medium. Hence, even for a layered structure composed of a thin film in which inner multireflection occurs as shown in Fig. 2(a), if we introduce an effective refractive index or an optically equivalent refractive index for the primary beam incidence to the equivalent bulk medium as shown in Fig. 2(b), it is possible to apply the model of Guosheng *et al.* to the layered structure. The effective refractive index was calculated as follows: The reflectivity coefficients of the equivalent bulk medium of Fig. 2(b)

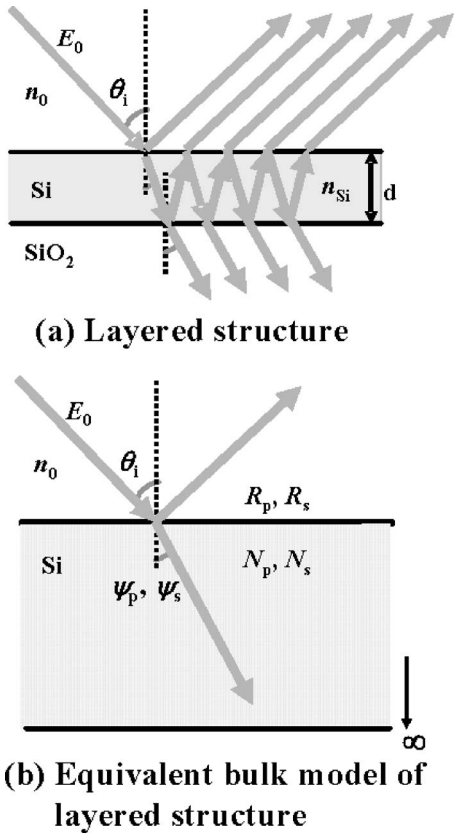

FIG. 2. Schematic drawings of (a) the actual layered structure sample and (b) its equivalent bulk model for the periodic E-D analysis. The reflected beam in (b) is the total of each individual reflected beam in (a). d is the film thickness, and n_0 and n_{Si} are refractive indices of the incident atmosphere and Si, respectively. R_i, N_i, and ψ_i are the overall reflectivity coefficient, equivalent refractive index, and equivalent refractive angle, respectively, where the subscript "i" is p or s to indicate p-polarized beam or s-polarized beam, respectively.

are set equal to the reflectivity coefficients of the layered structure of Fig. 2(a), R_p and R_s, where the subscripts p and s indicate p- and s-polarized beams, respectively. The R_i ($i=p$ or s) is derived by taking account of inner multireflected beams between the incident atmosphere/Si and Si/substrate. Using Snell's law, we can extract effective refractive indices N_p and N_s for the incident p- and s-polarized beams, as functions of R_p, R_s, and θ_i. The detailed derivation of N_p and N_s is mentioned in the Appendix. The calculation results using N_p and N_s showed that the E-D strongly depended on the film thickness due to the multireflection effect;[39] therefore, the multireflection effect must be considered in discussing the formation of periodic and aperiodic ridges.

Further, the refractive complex index of solid Si n_{Si} depends on temperature, and can be expressed as $4.153+5\times10^{-4}(T\text{-}300)\text{-}i0.038\exp[(T\text{-}300)/430)]$, where T (K) is the temperature of Si.[40] The temperature of the Si film increases rapidly due to pulse laser heating just after beginning the irradiation, then the Si film melts, and the temperature decreases quickly to room temperature.[41] For our experimental case, the irradiated Si film reaches a maximum temperature about 8 ns after irradiation, and cools down within 100 ns. Although, for strict analysis, this temperature dependence of n_{Si} should be taken into account for calculations of A and ϕ_p in P_n, we used the room temperature value of $4.153+i0.038$ as n_{Si} in order to simplify the calculation. Since it has been confirmed by calculation that A and ϕ_p are only slightly dependent on temperature, their values at room temperature are enough for discussion in this paper. Also, we mainly use the periodic E-D of the solid Si film because the periodic T-D in liquid Si is influenced strongly by the periodic E-D of the solid Si film, and is roughly proportional to it.

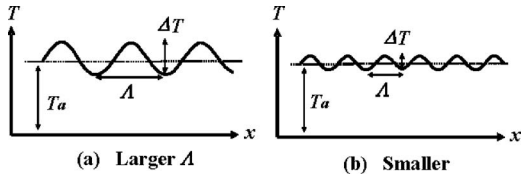

FIG. 3. Schematic drawings of the one-dimensional periodic temperature distributions on the irradiated Si film for (a) larger Λ and (b) smaller Λ, compared with the lateral thermal diffusion length in Si during irradiation. T_a is a spatial-average surface temperature, and ΔT is the difference in temperature between the maximum and the minimum in the periodic T-D.

C. Correction by thermal diffusion

We correct A in P_n with respect to the thermal diffusion in the Si film, because the periodic T-D does not perfectly correspond to the periodic E-D. Figures 3(a) and 3(b) show schematically the one-dimensional periodic temperature distributions of the surfaces of the irradiated Si films for the larger Λ and smaller Λ, respectively, compared with the lateral thermal diffusion length L_{th} of Si during irradiation. T_a is a spatial-average surface temperature, and ΔT is the difference in temperature between the maximum and minimum in the periodic T-D. If Λ is much larger than L_{th} during the pulse duration time, the reduction of the ΔT due to lateral thermal diffusion is negligible. On the other hand, if Λ is comparable to or smaller than L_{th}, the reduction of ΔT is not negligible. So, since A is not a decisive factor of the periodic T-D, it must be corrected.

For correction, we calculated the periodic T-D induced by the P_n of Eq. (2) by means of the two-dimensional finite difference heat transport equation, as follows:[42,43]

$$\rho\frac{h_{i,j}^{(t+1)}-h_{i,j}^{(t)}}{\Delta t}=\frac{1}{(\Delta x)^2}\left\{\frac{K_{i+1,j}+K_{i,j}}{2}[T_{i+1,j}^{(t)}-T_{i,j}^{(t)}]+\frac{K_{i,j}+K_{i-1,j}}{2}[T_{i-1,j}^{(t)}-T_{i,j}^{(t)}]\right\}+\frac{1}{(\Delta z)^2}\left\{\frac{K_{i,j+1}+K_{i,j}}{2}[T_{i,j+1}^{(t)}-T_{i,j}^{(t)}]+\frac{K_{i,j}+K_{i,j-1}}{2}[T_{i,j-1}^{(t)}-T_{i,j}^{(t)}]\right\}+S_{i,j}^{(t)}, \quad (3)$$

where Δx and Δz are very small dimensions along the x axis and z axis, respectively, $h_{i,j}^{(t)}$ is the enthalpy of a (i,j) cell with the area of $\Delta x\times\Delta z$ at time t, ρ is the density of the material, $K_{i,j}$ is the temperature-dependent thermal conductivity, $T_{i,j}^{(t)}$ is the temperature, and $S_{i,j}^{(t)}$ is the heat source term due to the absorption of the incident laser radiation. Basically, at every time step Δt, the model calculates the temperature profile of

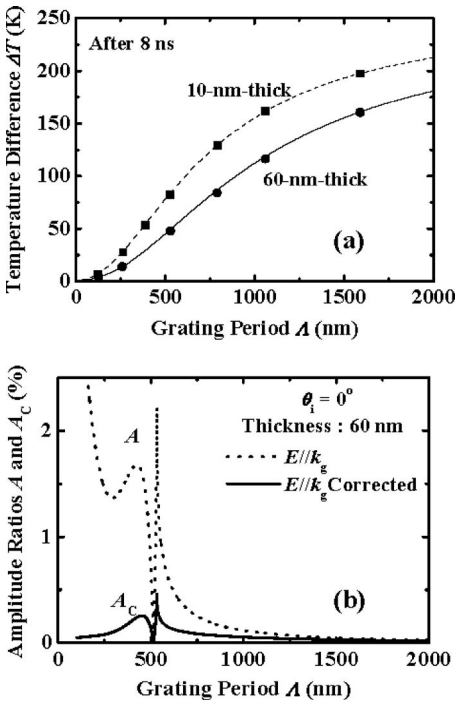

FIG. 4. (a) Grating period Λ dependences of the calculated temperature difference ΔT for 10- and 60-nm-thick Si films under the condition $h=1$ nm. The closed squares and dashed line indicate the calculated values and the fitting curve for the 10-nm-thick film, and the closed circles and solid line indicate the values and curve for the 60-nm-thick film. (b) Calculated dependences of amplitude ratio A (dotted line) and corrected amplitude ratio A_C (solid line) on grating period Λ for $\boldsymbol{E}\|\boldsymbol{k}_g$ at $\theta_i=0°$.

all cells, taking the profile of the pulse laser energy density into account. The details are mentioned in Ref. 43. In the calculation of Eq. (3), it was assumed that the primary incident beam energy profile with respect to the irradiation time, not space, was like a Gaussian with the full width at half maximum time of 6.5 ns and the total irradiation time of 13 ns, according to our experimental condition. Also, the temperature dependence of Si properties such as thermal conductivity[44] and refractive complex index of solid Si n_{Si} was considered. The n_{Si} was used for the calculation of the temperature dependences of the power reflection coefficient and power absorption. In practice, when ΔT was calculated, we adjusted the beam energy density to arrive at a value of T_a of 1280 °C at 8 ns after the start of irradiation. Since the calculated ΔT value does not include the rapidly transient phenomena from melting to solidification of the Si film, it is not adequate for estimating actual ΔT. However, the detailed analysis is very complicated and is not so valuable for this study. Also, the calculated ΔT value can be considered to include the essential physical phenomenon of thermal diffusion for our study of surface modification. In summary, in order to match the calculated periodic E-D to the actual periodic T-D as well as possible, we considered thermal diffusion which depends on the temperature-dependent thermal property, power reflection property, and optical absorption property of a crystal solid Si and also on the time after the beginning of irradiation.

Figure 4(a) shows the Λ dependences of the calculated temperature difference ΔT for 10- and 60-nm-thick Si films under the condition $h=1$ nm. The closed squares and dashed line indicate the calculated values and the fitting curve, respectively, for the 10-nm-thick film, and the closed circles and solid line are used in the same manner for the 60-nm-thick film. As can be seen from this figure, the ΔT for each case increases gradually with Λ and approaches a saturation value of ΔT_{sat} because the influence of lateral thermal diffusion on the temperature distribution is reduced with increasing Λ. The ΔT_{sat} of the fitting curves for the 10- and 60-nm-thick cases are 249 and 238 °C, respectively. On the contrary, for smaller Λ, the ΔT is further reduced, and ultimately becomes zero at $\Lambda=0$, which is equivalent to a flat temperature distribution. It can also be seen from Fig. 4(a) that the ΔT for 10 nm thickness is larger at any Λ, and saturates more quickly, than for 60 nm thickness. This means that the lateral heat diffusion in the 10-nm-thick film is less than the diffusion in the thicker film. According to this calculation result, we corrected A at any Λ by means of multiplying it by the correction factor, the ratio of $\Delta T/\Delta T_{sat}$. Here, we define a corrected ac amplitude ratio $A_C=A\Delta T/\Delta T_{sat}$.

Figure 4(b) shows the Λ dependences of the calculated amplitude ratios A and A_C for the case of $\boldsymbol{E}$ parallel to $\boldsymbol{k}_g$ at $\theta_i=0$, where the solid and dotted lines indicate A_C and A, respectively. As you can see from this figure, the A_C is greatly reduced with decreasing Λ, compared with A. This is because the amplitude with smaller Λ is more affected by thermal diffusion. Therefore, we must use the corrected amplitude A_C for the discussion of the mechanism of surface modification.

III. EXPERIMENT

a-Si films with thicknesses of 10 and 60 nm were deposited on Pyrex glass substrates at 350 °C in an ultrahigh vacuum chamber. Then, the Si film was transferred into another vacuum chamber, and was irradiated by a linearly polarized Nd:YAG pulse laser (wavelength of 532 nm, repetition frequency of 10 Hz, and pulse width of 6–7 ns) at room temperature. The other conditions in laser irradiation were as follows: For the 60-nm-thick Si film, the laser energy density F was 150 mJ/cm^2, which was not an average but a local value on the Gaussian profile, the irradiation pulse number N was 10, and the beam incident angles θ_i were 0°, 10°, or 20° with an *s*-polarized beam. For the 10-nm-thick Si film, the F was 70 mJ/cm^2, the N was 3000, and the θ_i were 0°, 8°, or 12° with an *s*-polarized beam. When the F was sufficient to melt the thinner Si film completely, the crystallized Si film was separated into many Si dots or islands randomly without a periodic structure on the glass substrate. In order to produce periodic structures such as a periodic line, the F was reduced low enough for only partial melting of the film. So, the pulse number for the 10-nm-thick film was much larger than that for the 60-nm-thick film. In the case of the *s*-polarized beam irradiation, the spatial periods Λ of the irradiated surface structures for $\theta_i=12°$ and 20° are expressed roughly as $\Lambda\approx\lambda/\cos\theta_i=1.022\lambda$ and 1.064λ, respectively, which are nearly equal to the wavelength of the laser

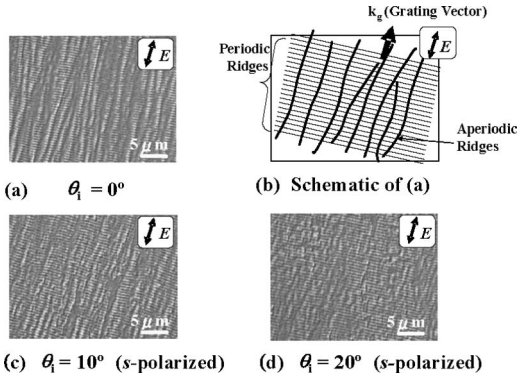

FIG. 5. Nomarski optical microscope images of surfaces of the 60-nm-thick Si films crystallized at θ_i=(a) 0°, (c) 10°, and (d) 20° with the *s*-polarized beam. (b) Schematic illustration of (a).

beam. The surface morphology was characterized by a Nomarski optical microscope and an atomic force microscope (AFM).

IV. RESULTS

Figures 5(a), 5(c), and 5(d) show the Nomarski optical microscope images of the surfaces of the Si films crystallized at θ_i=0°, 10°, and 20° with the *s*-polarized beam, respectively, and Fig. 5(b) shows the schematic illustration of Fig. 5(a). From Fig. 5(a), it can be seen that the fine ridges normal to $\boldsymbol{E}$ are aligned periodically with the spatial period $\Lambda \approx \lambda$ and that the grating vector $\boldsymbol{k}_\mathbf{g}$ of the ridge is perfectly parallel to $\boldsymbol{E}$, as shown schematically in Fig. 5(b). The root mean square (rms) of the height of the periodic ridges measured by AFM was roughly 30 nm, and the height was reduced by increasing the substrate temperature. In fact, we observed previously that the rms at the substrate temperature of 220 °C was less than 6 nm.[33,43] Also, in Fig. 5(a), it is noticed that many rugged ridges run roughly parallel to $\boldsymbol{E}$, and some collide with each other as shown schematically in Fig. 5(b). These are aperiodic ridges, as mentioned in Sec. I. Their height is not uniform, and the highest ridge is approximately 100 nm, which is obviously different from the periodic ridge. As shown in Figs. 5(c) and 5(d), the aperiodic ridges are gradually reduced with increasing θ_i, and almost disappear at θ_i=20°, but the periodic ridges still appear clearly as in the case of θ_i=0°. From this result, we can conclude that increasing θ_i to 20° is effective in suppressing the generation of aperiodic ridges.

Figures 6(a)–6(c) show the Nomarski optical microscope images of the 10-nm-thick Si films annealed at θ_i=0°, 8°, and 12°, respectively, with the *s*-polarized beam. In Fig. 6(a) at θ_i=0°, the periodic structures are hardly recognized, and each small rectangular Si island is roughly aligned parallel or perpendicular to $\boldsymbol{E}$. Because the Si film was so thin, 10 nm, the film tore apart during its melting. The many parts during the solidification process were agglomerated due to the surface tension of molten Si and its poor wetting on the substrate of SiO_2, which we observed, as shown in Fig. 6(a). The alignment direction of the Si islands will be discussed later in detail.

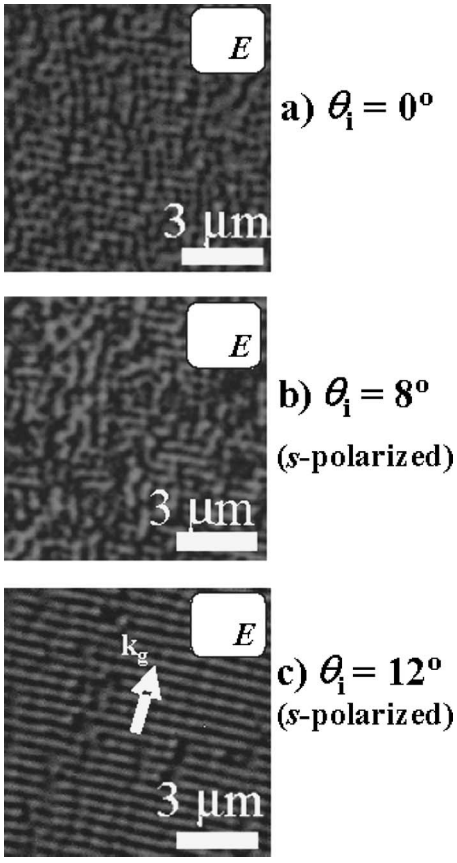

FIG. 6. Nomarski optical microscope images of surfaces of the 10-nm-thick Si films annealed at θ_i=(a) 0°, (c) 8°, and (d) 12° using the *s*-polarized beam.

As shown in Fig. 6(b) at θ_i=8°, although the directions of the islands are either parallel or perpendicular to $\boldsymbol{E}$, the ripped Si islands become longer, compared with the ones in Fig. 6(a). Further increasing θ_i to 12°, a number of Si stripes are periodically aligned perpendicular to $\boldsymbol{E}$ and the grating vector $\boldsymbol{k}_\mathbf{g}$ are parallel to $\boldsymbol{E}$, as shown in Fig. 6(c). Since the spatial period Λ of the Si stripes is roughly equal to λ, the formation is probably caused by the periodic E-D. According to the AFM measurement and the scanning electron microscope (SEM) observation, the height of the Si stripe was about 60 nm, and its shape was roughly half of a circular cylinder with a round top and flat bottom.

V. DISCUSSION

A. 60-nm-thick *a*-Si film

Figures 7(a) and 7(b) show the dependences of the corrected ac amplitude ratio A_C and phase ϕ_p of P_n, on the grating period Λ of the surface grating, where the Si film thickness is 60 nm, θ_i is 0°, and λ is 532 nm. The solid and dash lines indicate the cases of $\boldsymbol{E} \| \boldsymbol{k}_\mathbf{g}$ and $\boldsymbol{E} \perp \boldsymbol{k}_\mathbf{g}$, respectively. In this calculation, every Fourier component of the surface roughness of the Si film h before laser irradiation was set equal to 1 nm. We notice that the solid line for $\boldsymbol{E} \| \boldsymbol{k}_\mathbf{g}$ in Fig. 7(a) has a strong sharp peak around $\Lambda \approx \lambda$, at which ϕ_p=180° in Fig. 7(b). From this result, it is found that this ac component of P_n is enhanced by a positive feedback process

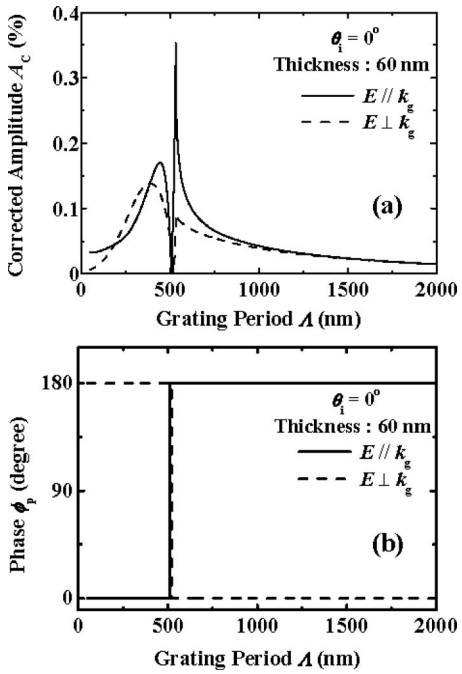

FIG. 7. Calculated dependences of (a) corrected amplitude ratio A_C and (b) phase ϕ_p of P_n on grating period Λ, where the Si film thickness is 60 nm, the incident angle θ_i is 0°, λ is 532 nm, and h is 1 nm. The solid and dash lines indicate the cases for $\boldsymbol{E}\|\boldsymbol{k}_g$ and $\boldsymbol{E}\perp\boldsymbol{k}_g$, respectively.

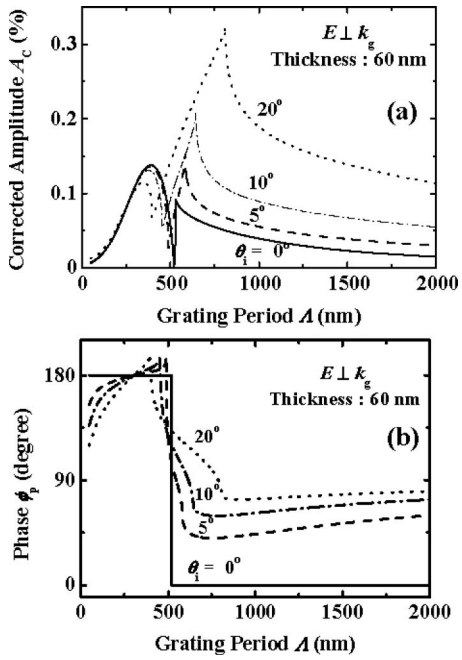

FIG. 8. Calculated dependences of (a) corrected amplitude ratio A_C and (b) phase ϕ_p on grating period Λ at θ_i of 0°, 5°, 10°, and 20°, where the film thickness of Si is 60 nm, h is 1 nm, and the primary incident beam with λ=532 nm is s-polarized with $\boldsymbol{E}\perp\boldsymbol{k}_g$.

as mentioned in Sec. II. In fact, we observed many periodic ridges (period λ) on the surface of the crystallized Si film, as shown in Fig. 5(a) at θ_i=0°.

On the other hand, for $\boldsymbol{E}\perp\boldsymbol{k}_g$, it can be seen from Figs. 7(a) and 7(b) that, at $\Lambda<500$ nm, the ϕ_p is 180°, which is favorable for periodic ridge formation, and that A_C has a peak. Although, from this calculation result, it can be expected that periodic ridge lines would be formed parallel to $\boldsymbol{E}$ or $\boldsymbol{E}\perp\boldsymbol{k}_g$, the aperiodic ridges were actually observed to be roughly parallel to $\boldsymbol{E}$ as shown in Fig. 5(a). We can explain this as follows: As shown in Fig. 7(a), the A_C for $\boldsymbol{E}\perp\boldsymbol{k}_g$ has a broad peak below Λ=500 nm, unlike that for $\boldsymbol{E}\|\boldsymbol{k}_g$, which means that resonance is not so strong and there is little positive feedback. Also, because the broad peak contains many kinds of large ac components which do not cancel out one another, many beats may occur due to interference among them. For example, when one component has Λ_1 =450 nm and the other has Λ_2=400 nm, the beat period $\Delta\Lambda$ between them is calculated to be 3.6 μm. Further, the beat waves interfere with one another and easily fluctuate, so that we observed aperiodic curvy ridges almost parallel to $\boldsymbol{E}$ as shown in Fig. 5(a). From Fig. 7, it can be said that the actual T-D in the irradiated Si film is not one dimensional with a coordinate parallel to $\boldsymbol{E}$ but two dimensional with two coordinates parallel and perpendicular to $\boldsymbol{E}$.

Next, we discuss the effect of tilting the incident beam on the reduction of the aperiodic ridge's height. Figure 8(a) shows the Λ dependences of the calculated A_C at θ_i of 0°, 5°, 10°, and 20° for $\boldsymbol{E}\perp\boldsymbol{k}_g$, where the incident beam is s polarized with $\boldsymbol{E}$ parallel to the ridges. As you can see from this figure, the A_C over Λ=500 nm increase with θ_i, while the values below Λ=500 nm decrease slightly. Also, we can see from the Λ dependence of ϕ_p in Fig. 8(b) that the ϕ_p below 500 nm is about 180°, and the ϕ_p over 500 nm is 45°–90°. Although the ac components of P_n with ϕ_p=45°–90° are unfavorable for a positive feedback process, increasing the amplitude of the ac components leads to destructive interference all over the range of Λ, so that no beat may occur. Therefore, it can be considered that the generation of the aperiodic ridges is suppressed with increasing θ_i, as shown in Figs. 5(c) and 5(d). On the other hand, for $\boldsymbol{E}\|\boldsymbol{k}_g$ in the case of oblique incidence, we can explain as follows: The diffraction efficiency for $\boldsymbol{E}\|\boldsymbol{k}_g$ is much larger and more resonant than that for $\boldsymbol{E}\perp\boldsymbol{k}_g$, as mentioned in Sec. II A. This is supported by the calculation result shown in Fig. 7(a), where the peak of A_C for $\boldsymbol{E}\|\boldsymbol{k}_g$ is much higher and sharper than that for $\boldsymbol{E}\perp\boldsymbol{k}_g$. Also, $\Lambda=\lambda/\cos 20° \approx 1.064\lambda$ is nearly equal to λ. Therefore, in the range of θ_i from 0° to 20°, the fine periodic ridges perpendicular to $\boldsymbol{E}$ with $\Lambda\approx\lambda$ were still formed, as shown in Fig. 5. This means that the T-D changed from two dimensional toward one dimensional by increasing θ_i.

B. 10-nm-thick *a*-Si film

Figures 9(a) and 9(b) show the Λ dependences of corrected amplitude ratio A_C and ϕ_p, respectively, for $\boldsymbol{E}\|\boldsymbol{k}_g$ and $\boldsymbol{E}\perp\boldsymbol{k}_g$ at normal incidence, where the film thickness of Si is 10 nm. We can see from Fig. 9 that the characteristics are much different from Fig. 7 for 60 nm thickness because of the multireflection effect. For the $\boldsymbol{E}\|\boldsymbol{k}_g$ case, it can be seen from this figure that ϕ_p is 0° in the range of $\Lambda>250$ nm although a strong and sharp peak appears around Λ =500 nm. So, it is possible to assume that the formation of the periodic structure is impeded by the negative feedback process. But, in fact, this assumption is not valid for the thinner film case, as mentioned later. For $\boldsymbol{E}\perp\boldsymbol{k}_g$, the ϕ_p for any Λ is 180°, which is favorable for periodic ridge forma-

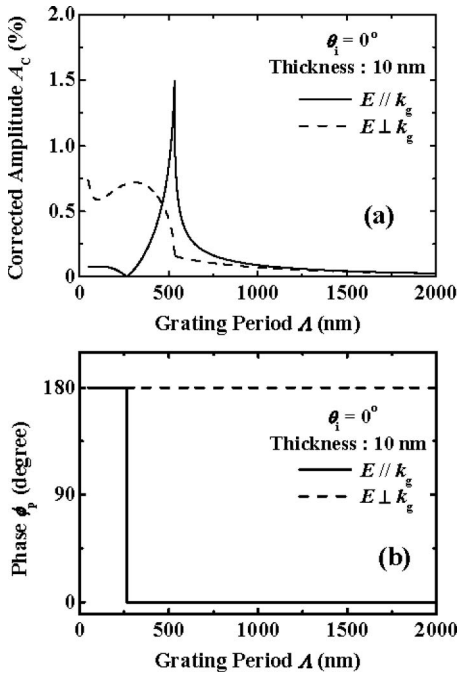

FIG. 9. Calculated dependences of (a) corrected amplitude ratio A_C and (b) phase ϕ_p on grating period Λ for $\boldsymbol{E}\|\boldsymbol{k}_g$ and $\boldsymbol{E}\perp\boldsymbol{k}_g$, where the film thickness of Si is 10 nm, θ_i is 0°, λ is 532 nm, and h is 1 nm. The solid and dash lines indicate the cases for $\boldsymbol{E}\|\boldsymbol{k}_g$ and $\boldsymbol{E}\perp\boldsymbol{k}_g$, respectively.

tion. However, the A_C does not have a strong resonant peak, and its characteristic to Λ is like a step function, in which the A_C is almost the same at all values below $\Lambda=500$ nm, and falls sharply over $\Lambda=500$ nm. Approximating the A_C-Λ characteristics for $\boldsymbol{E}\perp\boldsymbol{k}_g$ in Fig. 9(a) to a rectangular function in which $A_C=A_0$ for $|\Lambda|<\Lambda_0$ and $A_C=0$ for $|\Lambda|>\Lambda_0$ with $\Lambda_0 \approx 500$ nm and introducing new parameters of $k=2\pi/\Lambda$ and $k_0=2\pi/\Lambda_0$, we can calculate the ac term of the total energy density distribution $\Sigma P_{nac}(x)$ by superposing all the ac components of P_n with respect to k as

$$\Sigma P_{nac}(x) = \int_{k0}^{\infty} CA_0 \cos(kx)dk = CA_0\left[\delta(x) - \frac{\sin(k_0 x)}{x}\right], \tag{4}$$

where C is a constant. In deriving, we used Eq. (2), into which $\phi_p=180°$ was substituted according to Fig. 9(b). Since $\delta(x)$ is derived mathematically, it has no physical meaning and can be ignored. Equation (4) suggests that the E-D for $\boldsymbol{E}\perp\boldsymbol{k}_g$ should have a periodiclike component of $\Lambda_0=2\pi/k$ although $\Sigma P_{nac}(x)$ is not a strict periodic function. Also, because Eq. (4) shows the ac term in the E-D, not at the final irradiation stage, but at the initial one where any Λ exists with the same height on the irradiated surface, the positive feedback process of $\phi_p=180°$ can increase the height of the periodic Λ_0 with successive irradiation.

Based on the T-D expected from the above calculation results shown in Figs. 9(a) and 9(b), we speculate about the mechanism of the rectangular Si island formation, in which the rectangular-shaped Si islands are produced at the period of λ and are aligned parallel or perpendicular to $\boldsymbol{E}$, as shown in Fig. 6(a). In this speculation, we use the model proposed previously with respect to the formation of a pillar-shaped surface from a molten Si film.[32] Figure 10 shows the schematic diagram of the Si island formation process, where the F is adjusted to melt the Si film only partially. As shown in Fig. 10(a), a periodic E-D with the small amplitude produced by the first irradiation increases the surface roughness of the as-deposited Si film a little. For $\boldsymbol{E}\|\boldsymbol{k}_g$ with $\phi_p=0°$, the hills preformed with $\Lambda\approx\lambda$ induce a higher amplitude of P_n, however, the positions of the high energy density are not on the hills but in the valleys, as shown in Fig. 10(b), which creates new hills higher than the previous ones between each peak as shown in Fig. 10(c). The odd and the even numbers on the hills in Fig. 10(c) indicate the hills formed at the stages of Figs. 10(b) and 10(c), respectively. At each pulse, either the odd-numbered hills get taller or the even-numbered hills get taller, alternately. Then, one of the two hill groups is almost melted [Fig. 10(d)], and the molten regions are split near the center due to the surface tension and poor wetting to SiO_2

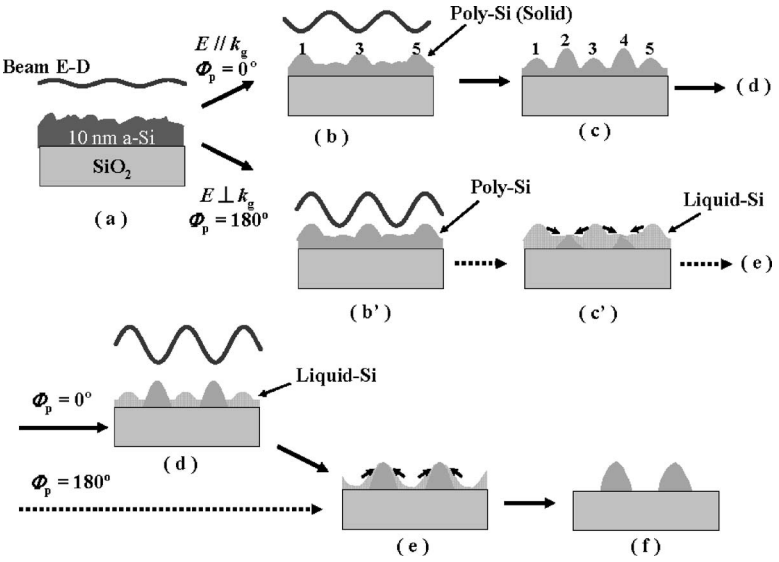

FIG. 10. Schematic diagram of the Si island formation process, where the beam energy density F is adjusted to melt the Si film not completely but partially. (a) as-deposited film, [(b), (c), and (d)] irradiated films for $\boldsymbol{E}\|\boldsymbol{k}_g$ and $\phi_p=0°$, [(b′) and (c′)] irradiated films for $\boldsymbol{E}\perp\boldsymbol{k}_g$ and $\phi_p=180°$, and [(e) and (f)] irradiated films for both $\boldsymbol{E}\|\boldsymbol{k}_g$ and $\boldsymbol{E}\perp\boldsymbol{k}_g$.

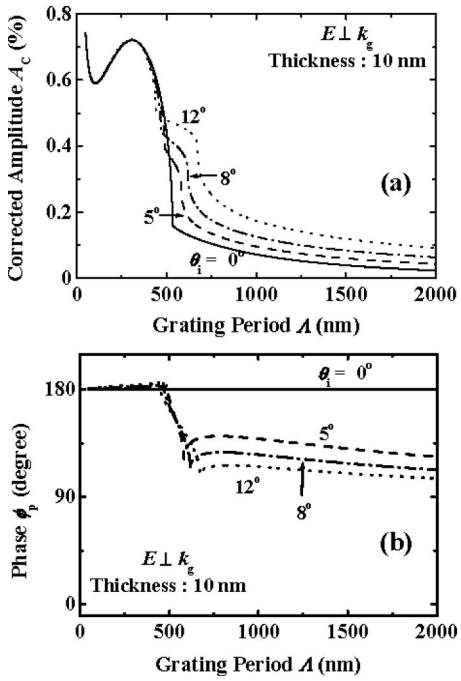

FIG. 11. Calculated dependences of (a) corrected amplitude ratio A_C and (b) phase ϕ_p on grating period Λ at θ_i of 0°, 5°, 8°, and 12° for $\boldsymbol{E} \perp \boldsymbol{k}_g$, where the film thickness of Si is 10 nm, h is 1 nm, and the primary incident beam with $\lambda = 532$ nm is s-polarized with $\boldsymbol{E} \perp \boldsymbol{k}_g$.

[Fig. 10(e)]. Eventually, each split part agglomerates around the respective neighboring nonmelted Si line region of the other hill group, and the size of the agglomerated hills becomes larger with the pulse number of irradiation as shown in Fig. 10(f).

For $\boldsymbol{E} \perp \boldsymbol{k}_g$ with $\phi_p = 180°$, the hills preformed with Λ_0 in Eq. (4) become larger and larger along with the pulse number because of the positive feedback loop process shown in Fig. 10(b′), as in the case of 60-nm-thick film. Then, the hills are molten from the top to bottom due to the larger amplitude of P_n, and the molten Si are split and drawn toward the nearest neighboring solid Si regions, as shown in Fig. 10(c′). After that, the Si film separates as in Figs. 10(e) and 10(f). As a result, due to the simultaneous progress of both the processes shown in Figs. 10(b) and 10(c), and Figs. 10(b′) and (c′), induced by the two-dimensional T-D, the continuous Si film is changed into a checklike pattern, and rectangular Si islands are formed with edges parallel or perpendicular to $\boldsymbol{E}$.

Next, we discuss the effect of tilting the incident beam on the formation of Si stripes from the 10-nm-thick Si film. Figure 11(a) shows the grating period Λ dependences of the calculated A_C at θ_i of 0°, 5°, 12°, and 20° for $\boldsymbol{E} \perp \boldsymbol{k}_g$. As you can see from these results, the A_C in the range of $\Lambda > 500$ nm increase with θ_i, which means that the periodiclike component of Λ_0 in Eq. (4) decreases with θ_i. This is because the A_C-Λ characteristics in Fig. 11(a) are distorted gradually with increasing θ_i from the rectangularlike function at $\theta_i = 0°$. Further, we can see from the Λ dependence of ϕ_p shown in Fig. 11(b) that the ϕ_p in the range of $\Lambda \geqslant 500$ nm decreases from 180° toward 90° with increasing θ_i. The components with $\phi_p = 90° - 135°$ do not undergo the positive feedback process. Eventually, because the diffraction efficiency of $\boldsymbol{E} \| \boldsymbol{k}_g$ is much larger and more resonant than that of $\boldsymbol{E} \perp \boldsymbol{k}_g$, and also because $\Lambda = \lambda / \cos 12°$ is nearly equal to λ, the molten Si film is not torn along the direction perpendicular to $\boldsymbol{E}$, and the Si line stripes with $\Lambda \approx \lambda$ are formed with $\boldsymbol{k}_g$ parallel to $\boldsymbol{E}$, as shown in Fig. 6(c) at $\theta_i = 12°$. That is, by increasing θ_i, the T-D is changed from two dimensional toward one-dimensional, as in the case of the 60-nm-thick film.

VI. CONCLUSION

We investigated the formation and suppression mechanisms of the aperiodic ridge, which depend on the incident angle θ_i of an s-polarized beam, on the surface of the 60-nm-thick Si film crystallized by irradiation using the linearly polarized Nd:YAG laser beam with $\lambda = 532$ nm. In the same way, we investigated the formation mechanisms of rectangular Si islands and linear Si stripes from continuous 10-nm-thick Si film, also. For this study, we improved the theoretical model of Guosheng *et al.* on periodic E-D, taking account of the multireflection effect in the Si film. Also, the calculation results were corrected with respect to thermal diffusion in the Si film during irradiation.

According to the calculation results, we proposed the mechanisms as follows: The aperiodic ridges on the 60-nm-thick Si film are formed by unstable beats in the molten Si film. These beats result from the constructive interference among some large ac components in a broad peak ($\Lambda < \lambda$) of the periodic E-D for $\boldsymbol{E} \perp \boldsymbol{k}_g$. By increasing the incident angle θ_i of the s-polarized beam from normal incidence, the beats are reduced due to the destructive interference among various large ac components which are generated over a wide range of Λ. It was found that, around $\theta_i = 20°$, the height of the aperiodic ridge was reduced, while the periodic ridge was still formed clearly. On the other hand, the shape and alignment direction of the islands which are produced from the 10-nm-thick Si film are governed by the ac components with $\Lambda \approx \lambda$ in the periodic E-D for both $\boldsymbol{E} \| \boldsymbol{k}_g$ and $\boldsymbol{E} \perp \boldsymbol{k}_g$. Since, by increasing θ_i of the s-polarized beam, the ac components in $\Lambda > \lambda$ for $\boldsymbol{E} \perp \boldsymbol{k}_g$ are enhanced, the special ac component with $\Lambda_0 \approx \lambda$ in Eq. (4) for $\boldsymbol{E} \perp \boldsymbol{k}_g$ is reduced due to the destructive interference. Then, at $\theta_i = 12°$, the continuous Si film is changed into separate linear stripes perpendicular to $\boldsymbol{E}$, which obeys the periodic E-D for $\boldsymbol{E} \| \boldsymbol{k}_g$.

In summary, by means of increasing θ_i of the s-polarized beam, the large ac component perpendicular to $\boldsymbol{E}$ at $\theta_i = 0$ in the E-D is reduced, thanks to the destructive interference among various ac components generated over a wide range in Λ. In other words, by increasing θ_i, the T-D in the irradiated Si film is changed from two-dimensional toward one dimensional. From this study, it can be concluded that the multireflection and thermal diffusion effects are important and essential factors for the surface modification of a Si film crystallized by the linearly polarized laser beam. This is because the multireflection effect strongly influences the amplitude and phase of every ac term, and the thermal diffusion during the heating of the irradiated film greatly reduces the amplitudes of the ac terms with Λ below the thermal diffusion length effectively.

APPENDIX

In this section, we present the detailed calculation method of the effective refractive indices N_p and N_s. Here, we assume that the reflected beam from the bottom of the glass substrate is neglected, as shown in Fig. 2(a). This is because the reflected power from the bottom of the substrate is less than 5% for $\theta_i \leqslant 20°$ and the thickness of the substrate is around 1 mm which is more than one thousand times the wavelength λ. The N_p, incident angle θ_i, and effective refractive angle ψ_p for the *p*-polarized incident beam are related to the total reflectivity coefficient R_p, taking multireflection into account, and the relation is given by

$$R_p = \frac{n_0 \cos \psi_p - N_p \cos \theta_i}{n_0 \cos \psi_p + N_p \cos \theta_i}, \tag{A1}$$

which is derived by elementary consideration of the continuity of the components of $\boldsymbol{E}$ and $\boldsymbol{H}$ parallel to the irradiated medium surface of Fig. 2(b). Combining Eq. (A1) with Snell's law of $n_0 \sin \theta_i = N_p \sin \psi_p$, and eliminating ψ_p, we obtain N_p as

$$N_p = \frac{n_0}{2\rho_p \cos \theta_i}\left(\sqrt{1 + 2\rho_p \sin \theta_i \cos \theta_i} + \sqrt{1 - 2\rho_p \sin \theta_i \cos \theta_i}\right), \tag{A2}$$

where $\rho_p \equiv (1+R_p)/(1-R_p)$. Similarly, for the *s*-polarized beam, using the total reflectivity coefficient R_s given by

$$R_s = \frac{n_0 \cos \theta_i - N_s \cos \psi_s}{n_0 \cos \theta_i + N_s \cos \psi_s}, \tag{A3}$$

and Snell's law of $n_0 \sin \theta_i = N_s \sin \psi_s$, we obtain N_s as

$$N_s = n_0 \sqrt{\left(\frac{\cos \theta_i}{\rho_s}\right)^2 + \sin^2 \theta_i}, \tag{A4}$$

where $\rho_s \equiv (1+R_s)/(1-R_s)$. Applying N_p and N_s as the refractive indices of the irradiated medium to the model of Guosheng *et al.*, we can obtain the E-D of the incident laser beam for the layered structure sample.

[1] T. Sameshima, S. Usui, and M. Sekiya, IEEE Electron Device Lett. **7**, 276 (1986).
[2] K. Sera, F. Okumura, H. Uchida, S. Itoh, S. Kaneko, and K. Hotta, IEEE Electron Device Lett. **36**, 2868 (1989).
[3] H. J. Kim and J. S. Im, Appl. Phys. Lett. **68**, 1513 (1996).
[4] M. Ozawa, C.-H. Oh, and M. Matsumura, Jpn. J. Appl. Phys., Part 1 **38**, 5700 (1999).
[5] A. Hara and N. Sasaki, Jpn. J. Appl. Phys., Part 2 **39**, L1 (2000).
[6] D.-H. Choi, K. Shimizu, O. Sugiura, and M. Matsumura, Jpn. J. Appl. Phys., Part 1 **31**, 4545 (1992).
[7] K. Shimizu, O. Sugiura, and M. Matsumura, IEEE Electron Device Lett. **40**, 112 (1993).
[8] R. Ishihara and P. Ch. van der Wilt, Jpn. J. Appl. Phys., Part 2 **37**, L15 (1998).
[9] L. Mariucci, R. Carluccio, A. Pecora, V. Foglietti, G. Fortunato, and D. D. Sala, Jpn. J. Appl. Phys., Part 2 **38**, L907 (1999).
[10] B. Rezek, C. E. Nebel, and M. Stutzmann, Jpn. J. Appl. Phys., Part 2 **38**, L1083 (1999).
[11] C.-H. Oh, M. Ozawa, and M. Matsumura, Jpn. J. Appl. Phys., Part 2 **37**, L492 (1998).
[12] Y. Taniguchi, M. Matsumura, M. Jyumonji, H. Ogawa, and M. Hiramatsu, J. Electrochem. Soc. **153**, G67 (2006).
[13] S. Horita, Y. Nakata, and A. Shimoyama, Appl. Phys. Lett. **78**, 2250 (2001).
[14] Y. Nakata, H. Kaki, and S. Horita, Mater. Res. Soc. Symp. Proc. **715**, 199 (2002).
[15] Y. Kawakami, E. Ozawa, and S. Sasaki, Appl. Phys. Lett. **74**, 3954 (1999).
[16] J. F. Young, J. S. Preston, H. M. van Driel, and J. E. Sipe, Phys. Rev. B **27**, 1155 (1983).
[17] C. T. Walters, Appl. Phys. Lett. **25**, 696 (1974).
[18] H. J. Leamy, G. A. Rozgonyi, T. T. Sheng, and G. K. Celler, Appl. Phys. Lett. **32**, 535 (1978).
[19] M. Oron and G. Sørensen, Appl. Phys. Lett. **35**, 782 (1979).
[20] P. M. Fauchet and A. E. Siegman, Appl. Phys. Lett. **40**, 824 (1982).
[21] J. F. Young, J. E. Sipe, J. S. Preston, and H. M. van Driel, Appl. Phys. Lett. **41**, 261 (1982).
[22] D. J. Ehrlich, S. R. J. Brueck, and J. Y. Tsao, Appl. Phys. Lett. **41**, 630 (1982).
[23] J. F. Young, J. E. Sipe, and H. M. van Driel, Phys. Rev. B **30**, 2001 (1984).
[24] I. A. Avrutskii, P. V. Bazakutsa, A. M. Prokhorov, and V. A. Sychugov, Sov. J. Quantum Electron. **15**, 429 (1985).
[25] J. S. Preston, H. M. van Driel, and J. E. Sipe, Phys. Rev. Lett. **58**, 69 (1986).
[26] P. E. Dyer and R. J. Farley, Appl. Phys. Lett. **57**, 765 (1990).
[27] Q.-H. Lu, X.-M. Lu, J. Yin, Z.-K. Zhu, Z.-G. Wang, and H. Hiraoka, Jpn. J. Appl. Phys., Part 1 **41**, 4635 (2002).
[28] A. E. Siegman and P. M. Fauchet, IEEE J. Quantum Electron. **22**, 1384 (1986).
[29] D. J. McCulloch and S. D. Brotherton, Appl. Phys. Lett. **66**, 2060 (1995).
[30] D. K. Fork, G. B. Anderson, J. B. Boyce, R. I. Johnson, and P. Mei, Appl. Phys. Lett. **68**, 2138 (1996).
[31] L. Mariucci, R. Carluccio, A. Pecora, V. Foglietti, G. Fortunato, and D. D. Sala, Jpn. J. Appl. Phys., Part 2 **38**, L907 (1999).
[32] A. Shin, C.-Y. Meng, and S.-C. Lee, and M.-Y. Chern, J. Appl. Phys. **88**, 3725 (2000).
[33] Y. Nakata, H. Kaki, and S. Horita, Jpn. J. Appl. Phys., Part 1 **43**, 2630 (2004).
[34] I. A. Avrutskii, P. V. Bazakutsa, A. M. Prokhorov, and V. A. Sychugov, Sov. J. Quantum Electron. **15**, 429 (1985).
[35] S. Horita, H. Kaki, and K. Nishioka, Digest of Technical Papers, 2005 International Workshop on Active-Matrix Liquid-Crystal Displays, Kanazawa, Japan, 6–8 July 2005, p. 179.
[36] J. E. Sipe, J. F. Young, J. S. Preston, and H. M. van Driel, Phys. Rev. B **27**, 1141 (1983).
[37] Z. Guosheng, P. M. Fauchet, and A. E. Siegman, Phys. Rev. B **26**, 5366 (1982).
[38] D. F. Edwards, in *Handbook of Optical Constants of Solids*, edited by E. D. Palik (Academic, San Diego, 1985), p. 547.
[39] S. Horita, H. Kaki, and K. Nishioka, Jpn. J. Appl. Phys., Part 1 **46**, 3527 (2007).
[40] G. E. Jellison, Jr., in *Semiconductors and Semimetals*, edited by R. F. Wood, C. W. White, and R. T. Young (Academic, Orlando, 1984), Vol. 23, p. 95.
[41] M. Hatano, S. Moon, and M. Lee, J. Appl. Phys. **87**, 36 (2000).
[42] R. F. Wood and G. A. Geist, Phys. Rev. B **34**, 2606 (1986).
[43] H. Kaki and S. Horita, J. Appl. Phys. **97**, 014904-1 (2005).
[44] C. J. Glassbrenner and G. A. Slack, Phys. Rev. **134**, A1058 (1964).